LA-UR -91-2103

LA-UR--91-2103

DE91 014591

Los Alamos National Laboratory is operated by the University of California for the United States Department of Energy under contract W-7405-ENG-36

TITLE The Deflagration-To-Degration Transition in Granular HMX

AUTHOR(S) J. M. McAfee
B. Asay
A. W. Campbell
J. B. Ramsay

SUBMITTED TO RCEM proceedings
Soccorro, NM
April 1991

DISCLAIMER

MASTER

Los Alamos Los Alamos National Laboratory
Los Alamos, New Mexico 87545

The Deflagration-to-Detonation Transition in Granular HMX

John McAfee, Blaine Asay, A. Wayne Campbell, and John Ramsay
Los Alamos National Laboratory
Los Alamos, New Mexico 87545

The early study of deflagration to detonation (DDT) was strongly influenced by the views of Kistiakowsky. His basic idea that convective burning could accelerate to detonation velocities formed the framework of many studies. There has been much speculation on how shock waves are formed by the burning explosive. Macek and Gipson hypothesized the reinforcement of pressure waves that results from coalescence of the u+c characteristics in cast explosives. Taylor suggested that convective burning plays a central role in bridging the gap between conductive burning and the transition to detonation.

The transition from deflagration to detonation in porous beds of explosive and propellant has received considerable attention both experimentally and theoretically. In many cases, the use of a hot-gas-producing igniter complicates the interpretation and subsequent modeling of experiments because considerable effort is required to account for the effect of the igniter gases on the granular bed. Hot-wire ignition is less intrusive; however, the ignition front is not planar. Thus the early events in these experiments cannot be approximated as one-dimensional.

Because of the complex nature of the early burning, we simplify the process of igniting the bed by pushing a combustion-driven piston into the lightly tamped HMX bed. HMX above the piston is ignited by the shear of and friction between particles. This ignition technique separates the early effects of igniter gas and conductive and convective burning that produce a weak compaction wave[5] in the bed from those processes at higher pressures that produce a more substantial compaction of the granulated bed. Our method of initiation also starts all processes in a single plane at one end of the tube.

We have studied the deflagration-to-detonation behavior of granular HMX confined in steel tubes with x-radiography, light emission, stress gauges, and various pin techniques. Simplification and consistency of results were obtained by igniting the HMX with a piston (initially at rest and in contact with the HMX) driven into the bed. A gasless igniter is used to start the burning of the piston propellant (low-density HMX) providing the piston with a smooth initial motion. Analysis of the data gives a detailed picture of the DDT process under these conditions. The qualitative and quantitative experimental results show the transition from burning to detonation is discontinuous. The results are discussed in terms of a descriptive model.

Deflagration to Detonation in Granular HMX

John M. McAfee
Blaine W Asay
A. Wayne Campbell
John B. Ramsay

Los Alamos National Laboratory
Los Alamos, New Mexico

presented to
Research Center for Energetic Materials
Open Seminar on Safety and Hazards Evaluation
April 9, 1991
New Mexico Tech, Socorro, New Mexico

Historically, the study of the deflagration-to-detonation transition is plagued with too many variables and not complete enough quantitative experimental information. In order to simplify experiments enough for understanding, A. Wayne Campbell (1980) developed a system of ignition using a slow piston (<100m/s) to give a planar and reproducible ignition to a well characterized granular bed of energetic material. He chose HMX because of the extensive body of information available on this explosive. One of his important results was determining that neoprene barriers placed in an experimental apparatus similar to the one used here did not change the distance-to-detonation in a tube. This proved that convection of hot burning gasses was not particularly important in DDT. Thus the planar ignition by piston does not change the basic mechanism of the process.

The approach at Los Alamos is to measure each experiment with as many diagnostics as possible. This allows the collection of enough information to sort out the complex structure of each test.

Experimental Requirements

Well Characterized Material:

Granular HMX (~150 μm dia.)

Reproducible and Planar Ignition:

Pressure-Driven Piston

Multiple, Simultaneous Diagnostics:

Radiography, Pins, Light Fibers (Emission, Reflectance Change), Stress Gauges, Microwave Interferometry

A typical piston-ignited DDT experiment is show here. The inset shows the O-ring-sealed piston above a burn chamber containing a measured amount of loosely packed HMX. This HMX is fired by an igniter consisting of a PyroFuse bridgewire and a mixture of Ti and B. The PyroFuse provides enough temperature to start the reaction $Ti + 2B \rightarrow TiB_2$, which provided enough temperature and energy to ignite the HMX in the burn chamber.

The typical tube is 7/8-in. outer diameter Maraging-steel tubing with a 1/2-in honed inner diameter.

Typical diagnostics are shown: coaxial ionization pins, capped-coaxial pins, burn-chamber pressure transducer, through-the-wall light fibers, and 0.005-in. thick Pb foils used as radiographic markers.

In order to establish the nomenclature used in this presentation, I have to describe the resultant model before going into the experimental evidence. The next two viewgraphs present the model.

Diagram **a** represents the initial condition of the experiment. The piston at rest and the granular bed of HMX at original density. For many experiments, initial density was 1.22 g/cc = 65% Theoretical Maximum Density (TMD) = 35% voids.

Diagram **b** is after the piston reaches full velocity. A compaction wave **c** proceeds up the tube. The condition behind is density of approximately 90% TMD.

Diagram **c** shows the compaction wave further up the tube. The wave **b** is an ignition wave that indicates the beginning of significant reaction (burning) in in the bed. The energy to start this wave comes from the friction between and the shear of the particles by the action of the compaction wave.

Diagram **d** shows the further progression of the compaction wave and the ignition wave. Additionally, and most importantly, another compaction region (near 100% TMD) forms in the tube above the ignition wave, but below the compaction wave. The origin of this wave is made clear in the next viewgraph. The upper boundary of the 100% region (named the "plug") develops to a shock **S**. The lower boundary is named the virtual piston **vp** because of its function in accelerating the shock.

Diagram **e** shows the shock at a later time running faster in the 90% compact. Notice the burning of the material below the virtual piston. The ignition wave essentially stops when it reaches the plug (100% TMD region) because the linear burn rate drops by over a factor of 20 between 90% and 100% TMD. On the time scale of the process, this amounts to a stoppage.

Diagram **f** shows the time after which the shock was strong enough to initiate detonation by a normal shock-to-detonation. The detonation velocity is characteristic of the original density material after the compaction wave is overtaken.

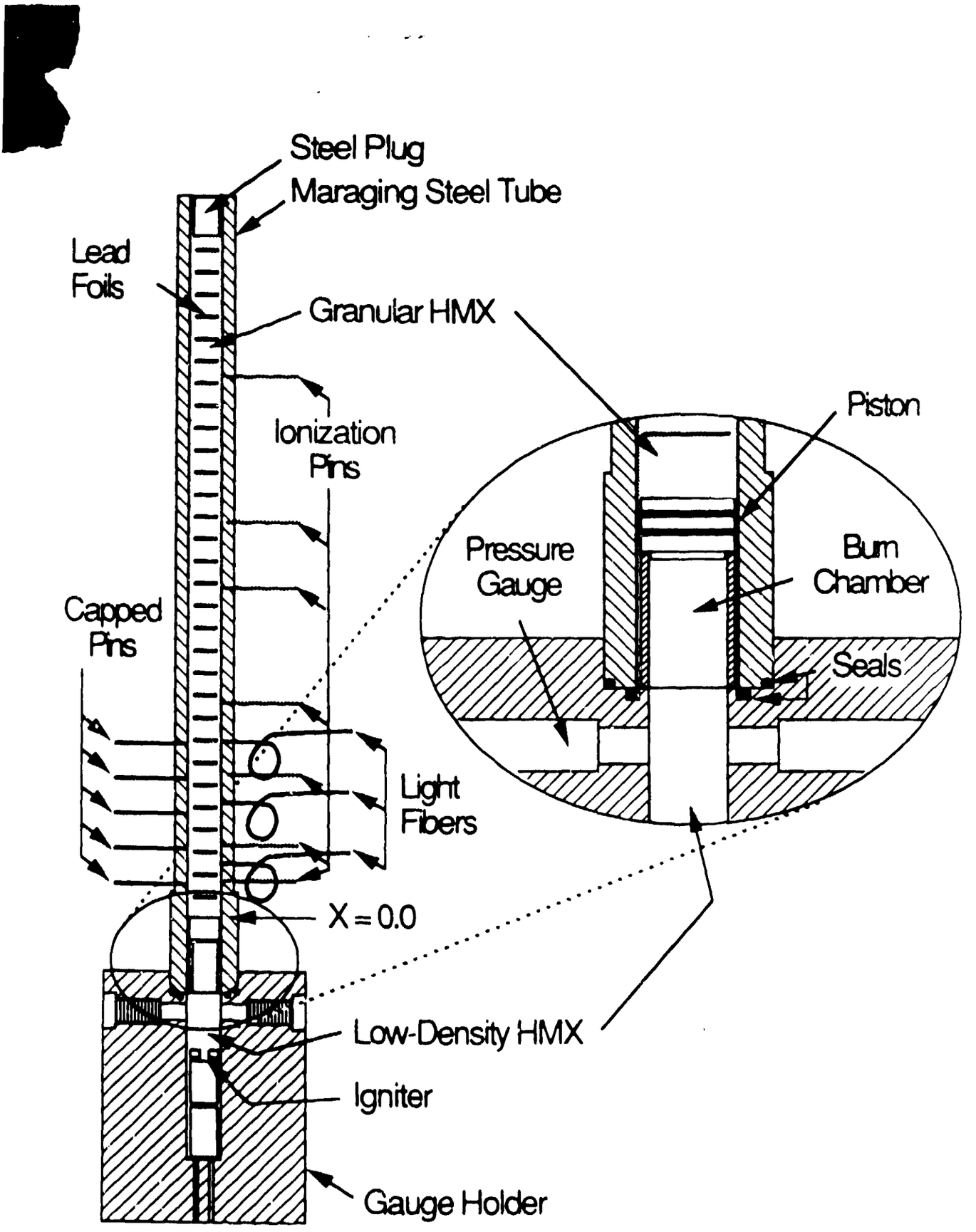
Steel Plug
Maraging Steel Tube
Lead Foils
Granular HMX
Ionization Pins
Piston
Pressure Gauge
Burn Chamber
Capped Pins
Seals
Light Fibers
X = 0.0
Low-Density HMX
Igniter
Gauge Holder

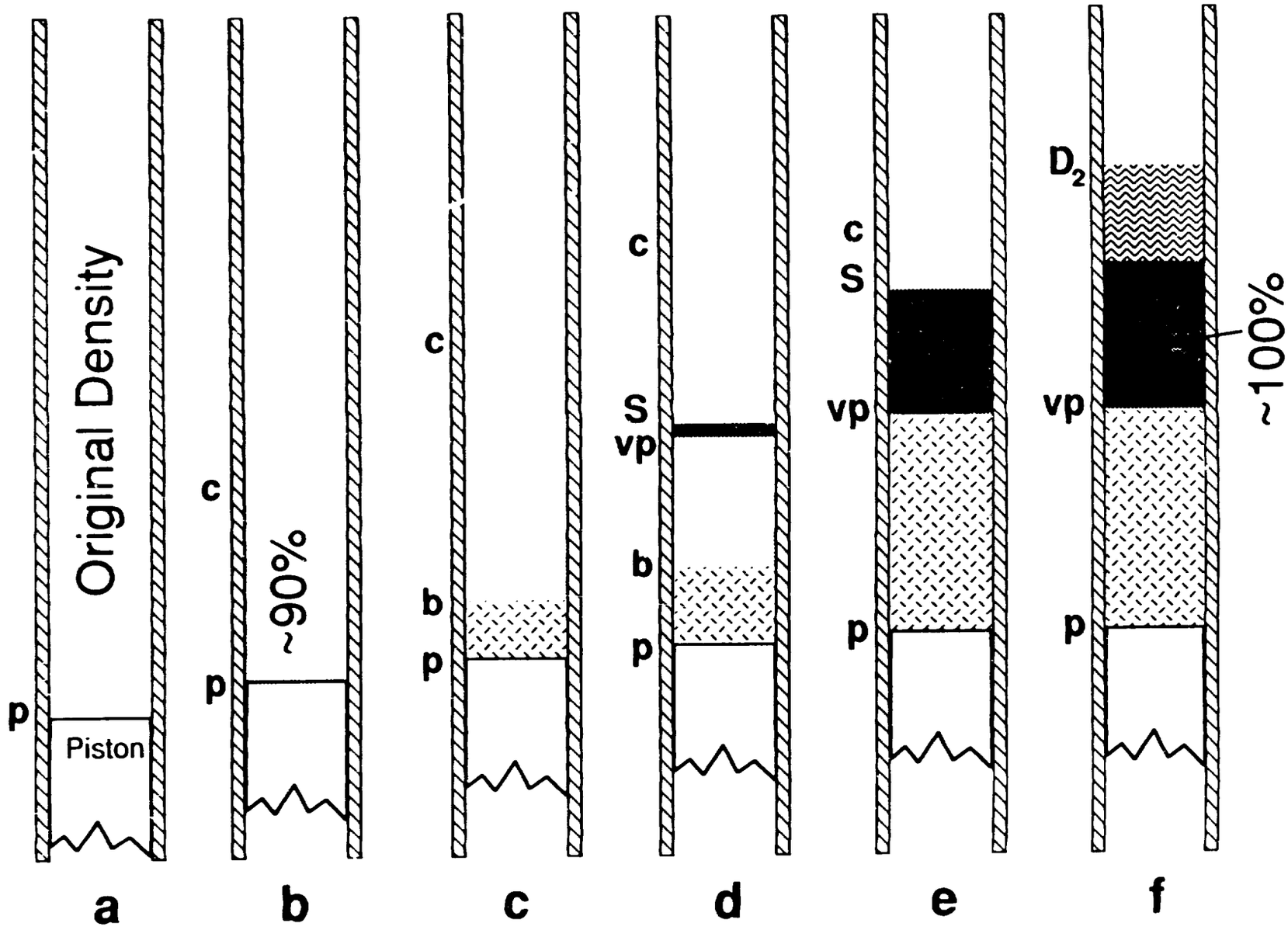
Original Density
p
Piston
a
c
~90%
p
b
c
b
p
c
S
vp
b
p
d
c
S
vp
p
e
D2
c
S
vp
p
~100%
f

This diagram shows the DDT mechanism in the time-distance plane. The additional information shown is the approximate trajectory of stress waves σ_i that originate from the higher pressures generated in the bed by the burning behind the ignition wave. The increase in the sound speed in the compact with pressure allows the coalescence of a set of these stress waves. This coalescence of stress further collapses the 90% TMD bed to near 100% TMD. This is the beginning of the plug. When the ignition wave **b** reaches the bottom of the 100% TMD material, it essentially stops because of the difference in burn rate. The increasing pressure in the burning region accelerates the **vp**, which, in turn, more strongly accelerates the shock **S**. When the shock is strong enough, a shock-to-detonation transition takes place in the 90% compact. The initial detonation runs at the velocity characteristic of the 90% compact $\mathbf{D_1}$. The detonation slows to the velocity characteristic of the original bed $\mathbf{D_2}$ when it overtakes the compaction wave.

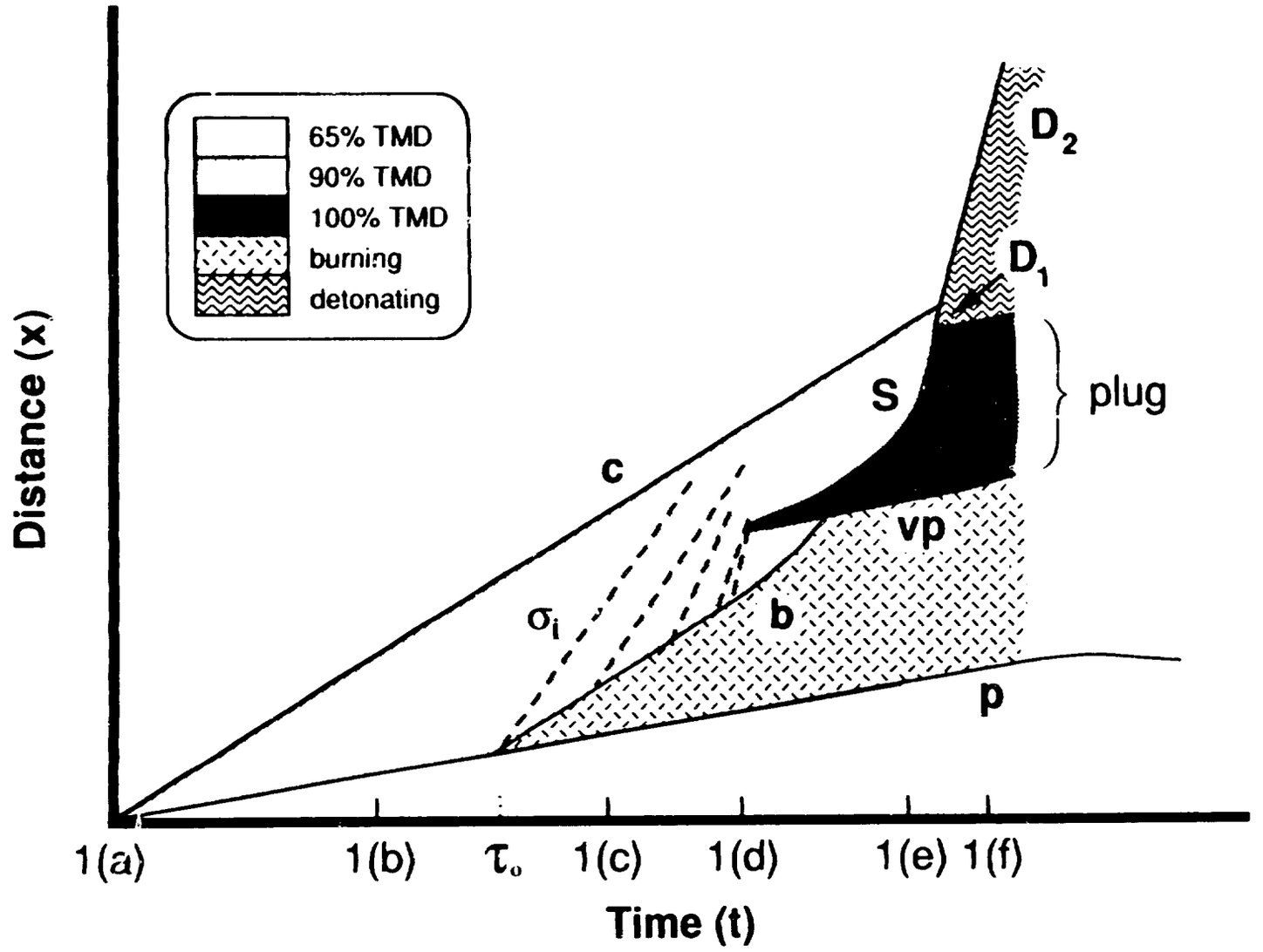
65% TMD
90% TMD
100% TMD
burning
detonating
Distance (x)
D2
D1
S
plug
c
vp
σi
b
p
1(a)
1(b)
τo
1(c)
1(d)
1(e)
1(f)
Time (t)

This t-x diagram shows all the information in the previous diagram. The additional information is typical particle paths, 1^{st}, i^{th}, and j^{th}. The acceleration of the ignition wave is caused by the effect of the stress waves on particles at different positions in the tube.

The thermal decomposition of HMX is kinetically autocatalytic. This means the rate of reaction is very slow at first, and increases rapidly after an induction period τ_0. Some interesting details of autocatalysis are given near the end of this presentation. This rapid increase in reaction rate defines the position of the ignition wave **b**. The induction period for the 1^{st} particle is determined by the decomposition caused during the compaction by wave **c**. Further up the tube, the i^{th} particle is compacted at a later time. If the stress waves had no effect on the kinetics of decomposition, the induction period to ignition would be exactly τ_0. However, the stress waves provide additional reaction products. Therefore, because of the dependence of the induction period on the product concentration, the total time between the compaction wave and the ignition is shorter than τ_0. The j^{th} particle is affected by the stress waves over a longer time than particles below it. Therefore, its induction period is still shorter. Thus the trajectory of the ignition wave accelerates relative to the compaction wave.

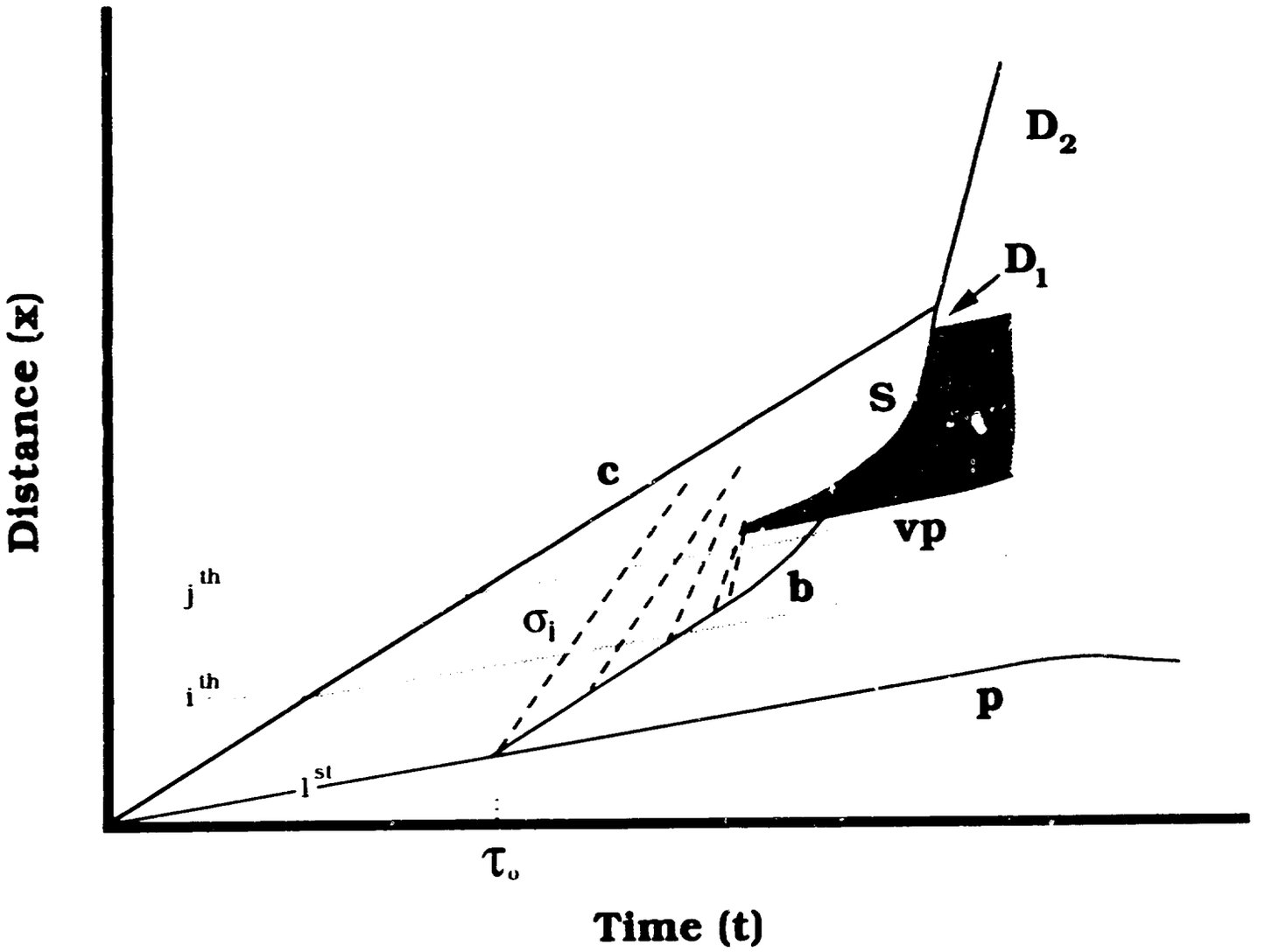
Distance (x)
D2
D1
S
c
vp
b
σi
j th
i th
p
l st
τo
Time (t)

This viewgraph begins the recitation of the experimental evidence for the descriptive model.

The first waves considered are the compaction wave and the stress waves. The best measurements of these waves are given in this viewgraph. The three traces are the record from a strain-compensated Manganin gauge placed in a tube at a position where it would intercept first the compaction wave, then the plug. The gauge trajectory is above the j^{th} particle shown in the previous viewgraph. Curve **a** is the entire record at low vertical resolution. Curve **b** concentrates on the compaction wave. After initial compaction, the stress condition is relatively constant until the increase at approximately 385 μs. This rise is attributed to the increased compaction from the stress waves. The rapid rise after 395 μs is the entrance of the gauge into the plug region. Curve **c** is a detail of the plug measurements.

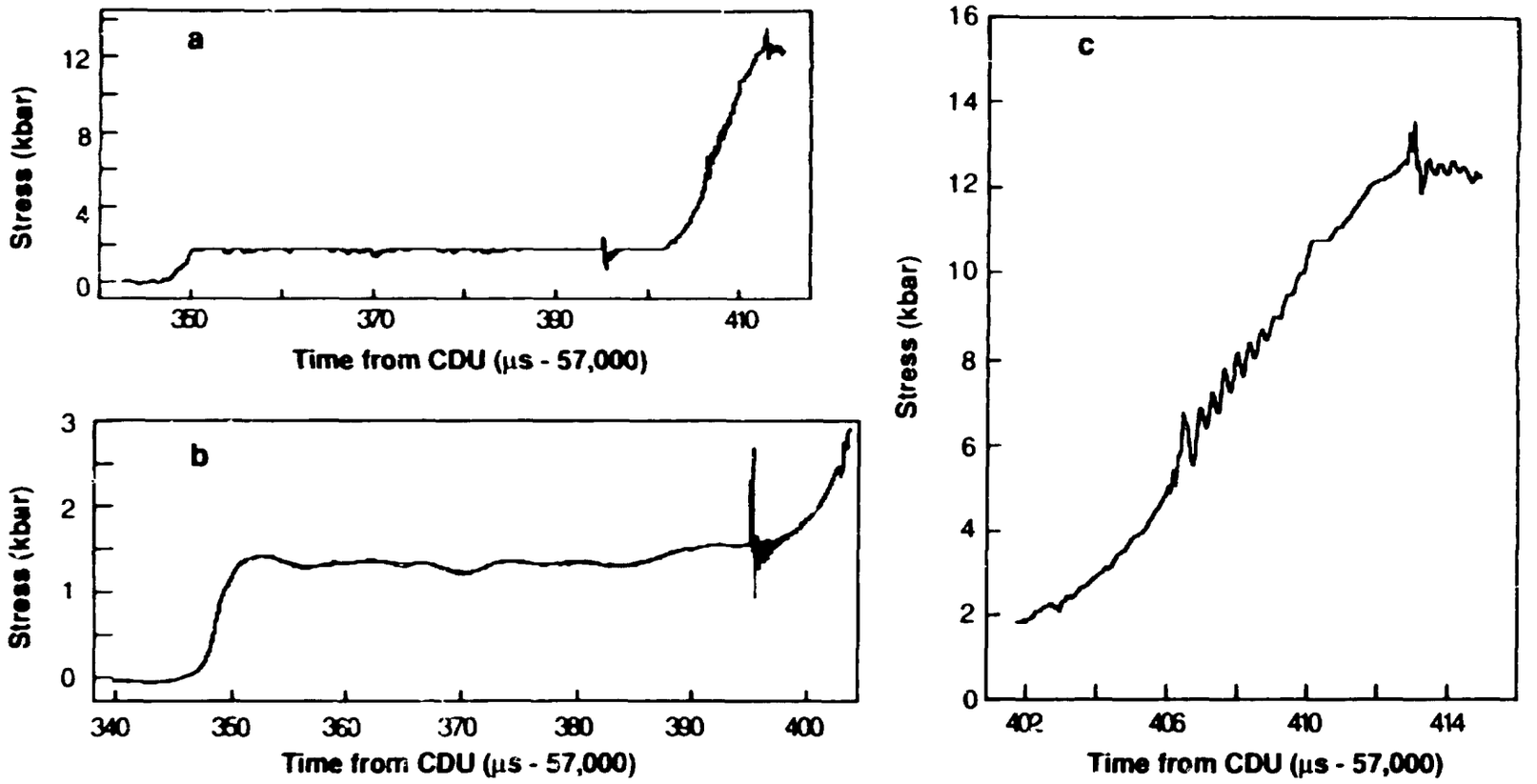
a
Stress (kbar)
0
4
8
12
360
370
390
410
Time from CDU (μs - 57,000)
b
Stress (kbar)
0
1
2
3
340
350
360
370
380
390
400
Time from CDU (μs - 57,000)
c
Stress (kbar)
0
2
4
6
8
10
12
14
16
402
406
410
414
Time from CDU (μs - 57,000)

Measuring the profile of the compaction wave is important in order to determine the dynamic material properties of the granular bed. The Manganin gauge record on the previous viewgraph gave the compaction-wave profile in detail. We wished to measure the profile with an independent diagnostic. We did this by developing a Helium-Neon-Laser Reflectometer.

A diagram of this apparatus is shown. The principle of measurement is the change in diffuse reflectance of the granular bed with compaction.

The laser light is linearly polarized before being focused into a silica light fiber. The fiber penetrates the steel DDT tube wall, and is placed flush with the inner wall. A low-level signal is returned from the diffuse reflection of the HMX bed. The return signal is discriminated from the bright probe light reflections by another polarizer (the analyzer) placed at 90° to the initial polarization. The recorded signal is a measure of the reflecting properties of the HMX at the end of the fiber.

We expected the reflected light to increase with the compaction of the HMX bed.

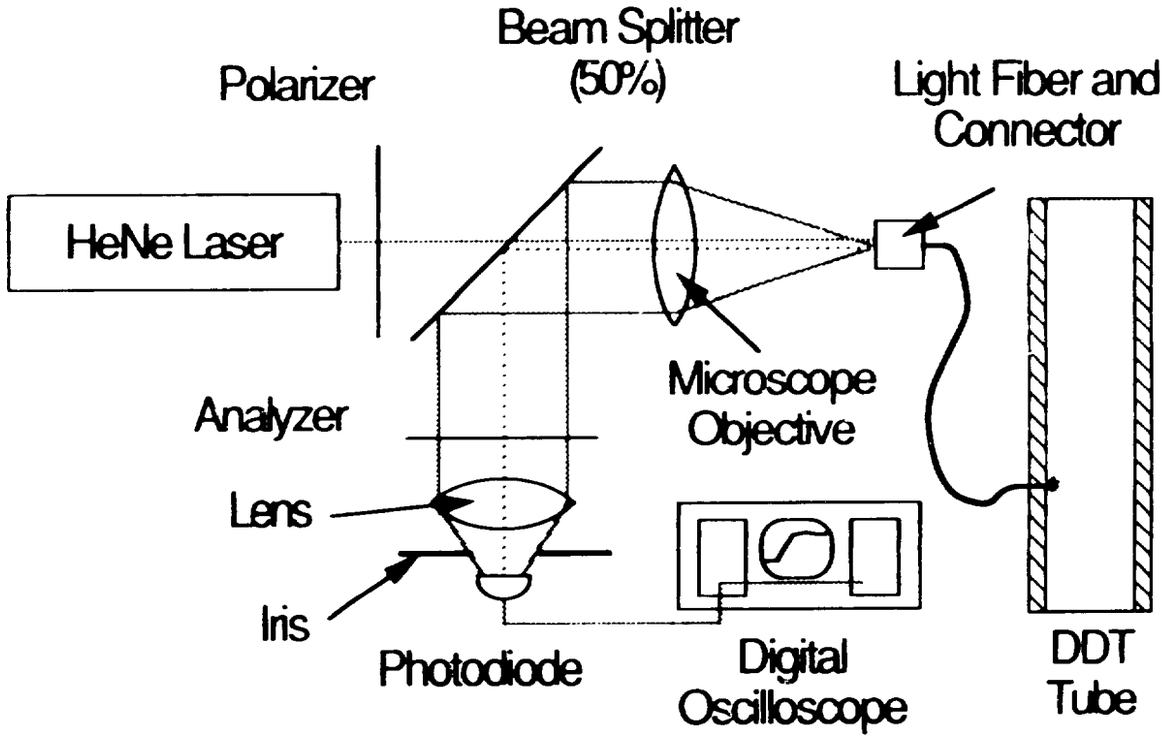
Beam Splitter
(50%)
Polarizer
Light Fiber and
Connector
HeNe Laser
Microscope
Objective
Analyzer
Lens
Iris
Photodiode
Digital
Oscilloscope
DDT
Tube

These traces are a superposition of the compaction-wave profiles recorded by a Manganin gauge and the laser reflectometer in the same experiment. The signals are normalized in amplitude and shifted in time to show the best comparison. The profiles are quite similar, thus indicating each is a good measurement of the profile.

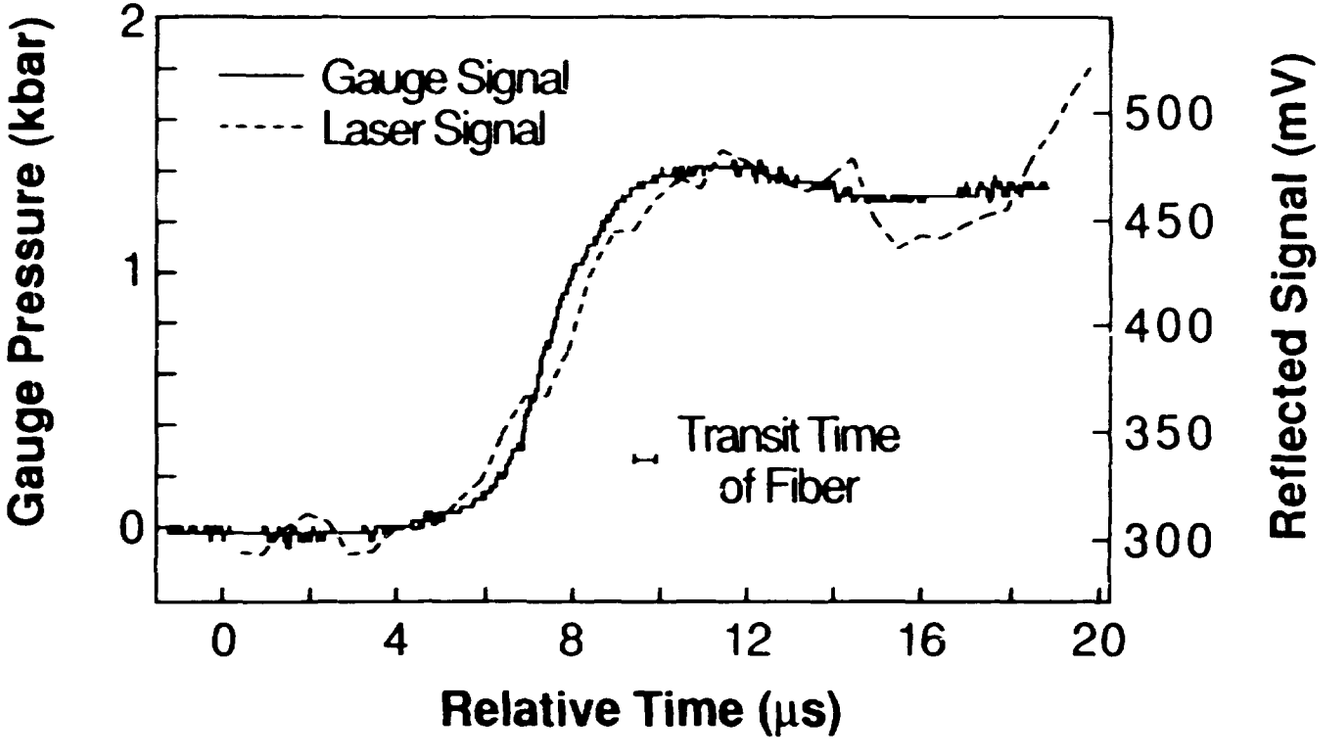
Gauge Signal
Laser Signal
Transit Time
of Fiber
Gauge Pressure (kbar)
Reflected Signal (mV)
Relative Time (μs)
0
1
2
300
350
400
450
500
0
4
8
12
16
20

The next wave considered in the descriptive model is the ignition wave **b**.

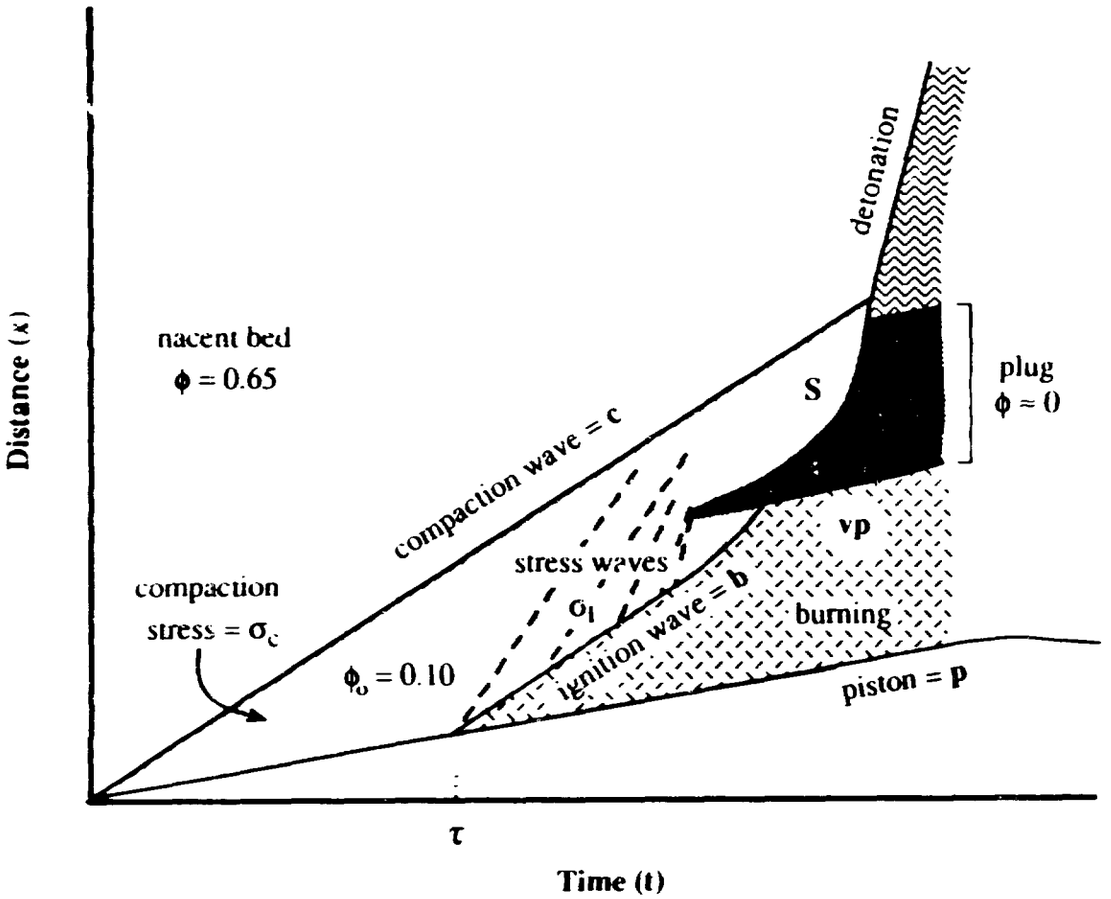
Distance (x)
nacent bed
$\phi = 0.65$
compaction wave = c
detonation
S
plug
$\phi \approx 0$
vp
stress waves
σ_i
ignition wave = b
burning
compaction
stress = σ_c
$\phi_o = 0.10$
piston = p
τ
Time (t)

The particular experiment that best defined the ignition wave is diagrammed. In addition to the ionization and capped pins, and the radiographic marker-foils, three light fibers were placed through the tube wall. These fibers were only observatory. Light emitted from the bed and intercepted by the fiber ends was recorded by a matched set of amplifiers (6 MHz bandwidth).

The diagram on the right shows the regions of observation as shown by the radiography.

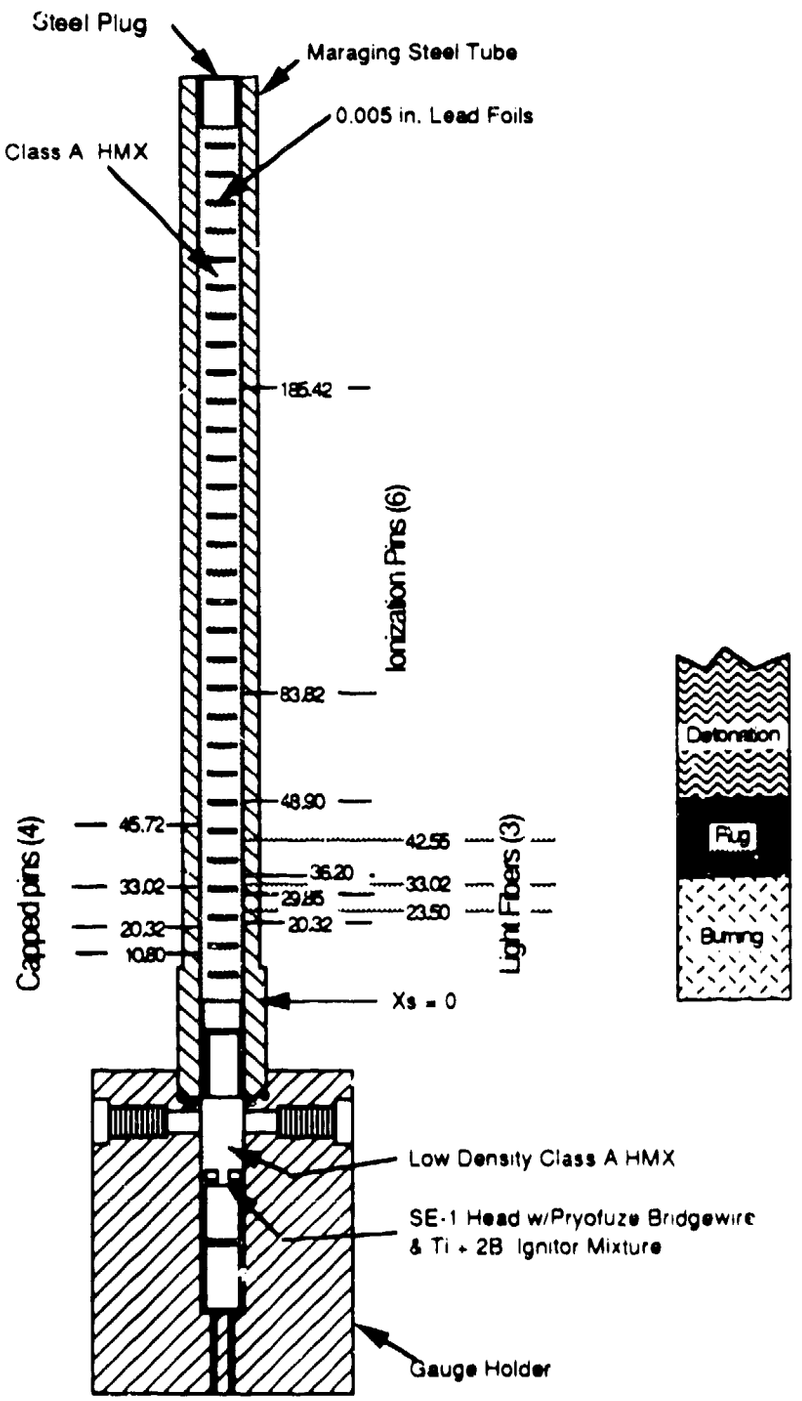
Steel Plug
Maraging Steel Tube
0.005 in. Lead Foils
Class A HMX
185.42
Ionization Pins (6)
83.82
48.90
Capped pins (4)
45.72
42.55
36.20
33.02
29.85
33.02
23.50
20.32
20.32
10.80
Light Fibers (3)
Xs = 0
Detonation
Rig
Burning
Low Density Class A HMX
SE-1 Head w/Pryofuze Bridgewire
& Ti + 2B Ignitor Mixture
Gauge Holder

Shot E-5586

The signals recorded from the three light fibers are shown. The first two fibers recorded quite similar signals. Each has a very fast rise and a near constant amplitude until detonation (after 240 μs). The third signal is qualitatively distinct. The first indication is the low-level "toe," followed by a slower rise, a point of inflection near the amplitude of the other fiber signals, and an excursion to a higher level.

The qualitative difference between the first two fiber signals and the third is evidence for two distinct regions. In the lower region (fibers #1 and #2), the fast rising signal and constant intensity indicate ignition and light emission from a constant temperature. The more complex third signal could only be interpreted in conjunction with the other data from this experiment shown on the next viewgraph.

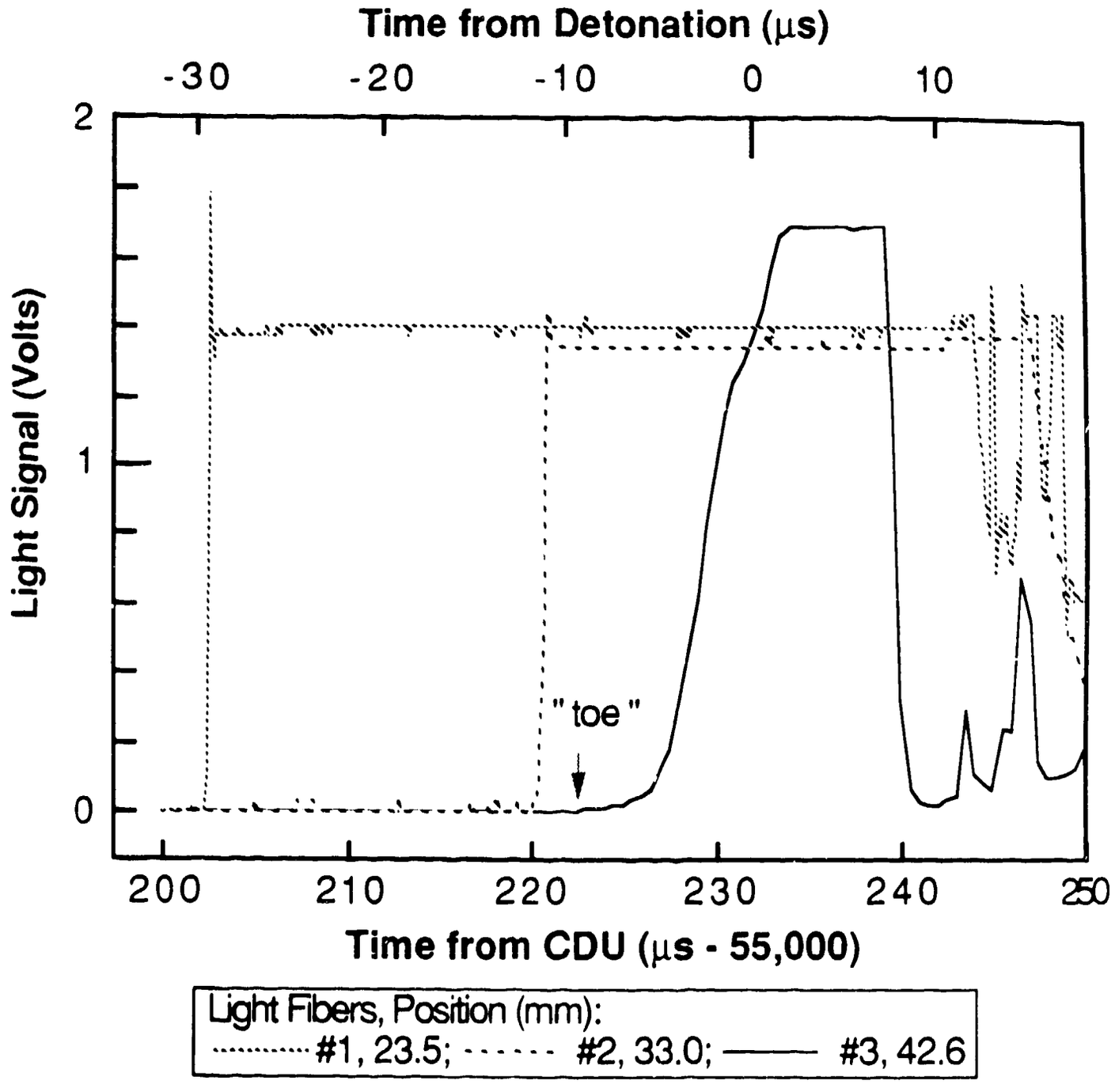
Time from Detonation (μs)
-30
-20
-10
0
10
2
1
0
Light Signal (Volts)
" toe "
200
210
220
230
240
250
Time from CDU (μs - 55,000)
Light Fibers, Position (mm):
#1, 23.5; #2, 33.0; #3, 42.6

This compilation of results is a t-x representation of the pin, radiographic, and light-fiber data consistent with the description of the DDT process. The compaction wave trajectory is extrapolated from capped pin reports (some not shown). The piston trajectory is from radiography (see examples in later viewgraphs). The light-fiber data are represented by the horizontal lines labeled #1, #2, and #3. The length of the lines for fibers #1 and #2 corresponds to the constant intensity portion of the signals. The signal from fiber #3 is represented by two segments: The early segment starts at the "toe" and ends at the inflection point. The later segment starts at the inflection and ends at the signal drop.

The leading edges of the first two fibers map the ignition-wave trajectory. The velocity between these points is faster than that of the compaction wave, as the description would indicate.

The third fiber can only be interpreted by using the ionization-pin reports and the radiography results. The ionization pins report at some low level of conductivity. Their reports indicate first significant reaction in the bed. By connecting the pin points at ~200 μs and ~230 μs with the "toe" of the third light signal, we can trace the trajectory of the shock S. The location of the shocked region (i.e., the ~100% TMD region) is found from radiographic data.

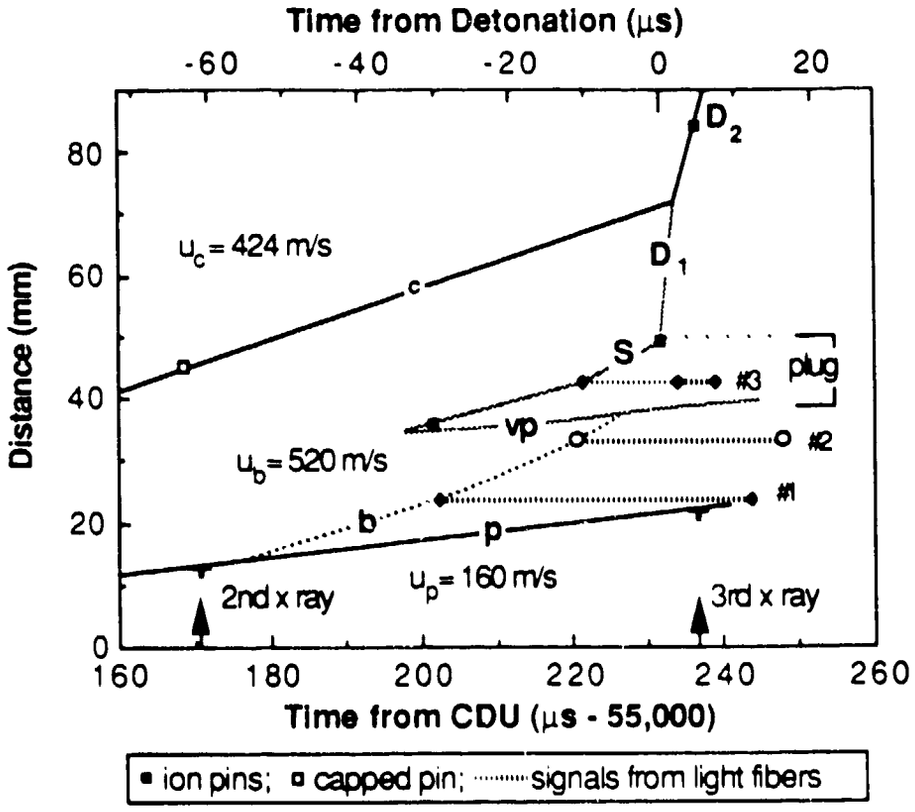
Time from Detonation (μs)
-60
-40
-20
0
20
Distance (mm)
80
60
40
20
0
D_2
D_1
u_c = 424 m/s
c
S
plug
#3
vp
#2
u_b = 520 m/s
b
#1
p
u_p = 160 m/s
2nd x ray
3rd x ray
160
180
200
220
240
260
Time from CDU (μs - 55,000)
ion pins; capped pin; signals from light fibers

The radiographic measurements of the "plug" or shocked region were essential to the development of this description of the DDT process

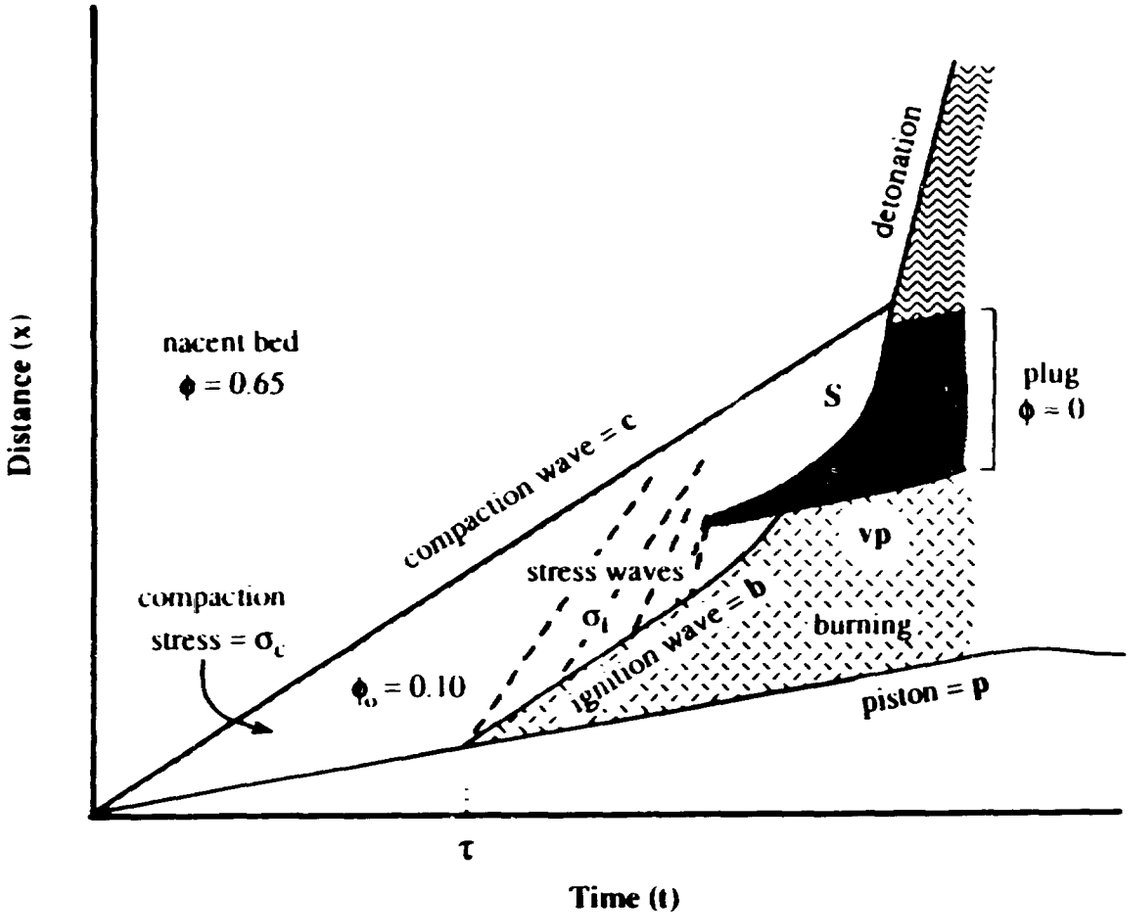
Distance (x)
nacent bed
$\phi = 0.65$
compaction wave = c
compaction
stress = σ_c
$\phi_o = 0.10$
stress waves
σ_i
ignition wave = b
S
detonation
plug
$\phi = 0$
vp
burning
piston = p
τ
Time (t)

The four radiographs in this viewgraph show, respectively, the positions of the Pb foil markers before the experiment and at three later times.

The first dynamic radiograph shows the piston moving into the tube and the compression of the material between the first four foils.

The second dynamic radiograph shows additional compression between foils 3-6. The piston and foils 1 and 2 have moved further apart than in the first dynamic. Slight bulging at the piston end of the tube indicated higher pressure in the region of the piston and foils 1 and 2.

The third dynamic radiograph was taken after the transition to detonation. The detonation is just beyond foil 11. The highly compressed region between foils 2-6 is still evident. The wall distortion on the piston end is more visible. Additionally, the conical distortion diagnostic of detonation is visible from foils 6-11. The tube is less expanded in the compressed region, indicating either lower pressure or a fast transit of high pressure without gas (working fluid) production. The second interpretation is preferred. This is the plug or shocked region. As in the classic description of shock-to-detonation (SDT), the run-up shocked material remains relatively intact after detonation.

STATIC

FIRST DYNAMIC

SECOND DYNAMIC

THIRD DYNAMIC

M-8 SHOT B-9153

This viewgraph plots the quantitative results of analysis of the previous radiographs and two additional radiographs from a different experiment. Distance along the tube relative to the at-rest piston position is plotted against HMX density. The original bed density was ~65% TMD.

Plot **a** shows the compaction wave with the density ~90% TMD. There is no indication of extensive reaction between the piston and the head of the wave.

Plot **b** was taken approximately 2 μs before the transition to detonation. The near 100% TMD region from ~33 to ~50 mm is the plug. From the piston to ~27 mm, the density has dropped from the 90% compaction value.

Plots **c**, **d**, and **e** are from radiographs taken after detonation. The detonation moves further down the tube in each plot. The plug region remains relatively intact. The region between the plug and the piston shows decreasing density, consistent with the high temperature-high pressure gas from the burning region. The density measurements take into account the distortion of the tube shown in the radiographs.

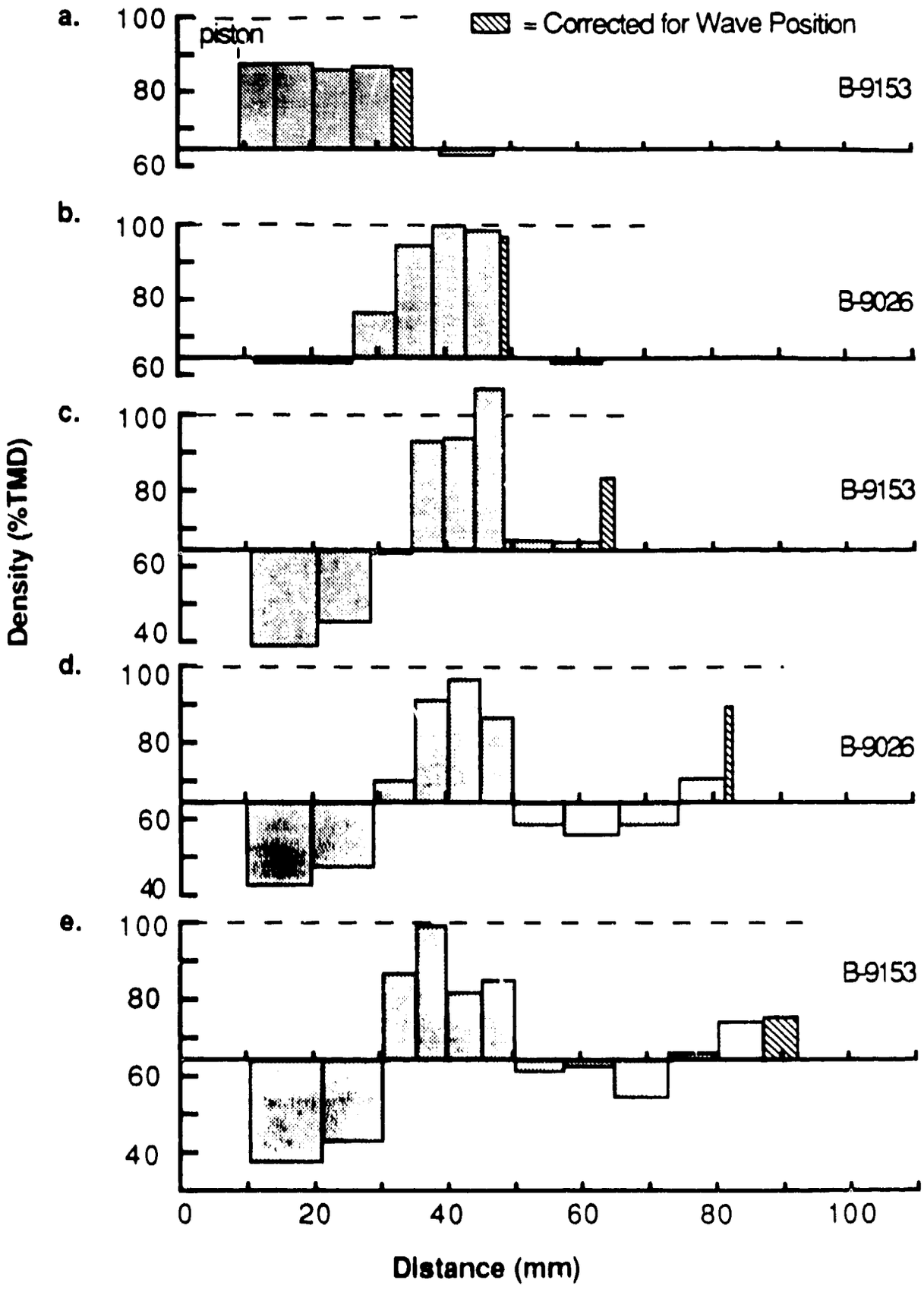
a.
b.
c.
d.
e.
100
80
60
40
piston
= Corrected for Wave Position
B-9153
B-9026
B-9153
B-9026
B-9153
Density (%TMD)
0
20
40
60
80
100
Distance (mm)

The next viewgraph gives a compilation of data from an typical experiment. In addition to the various wave trajectories measured by different types of pins, the pressure in the burn chamber (behind the piston) is given.

Note where the compaction wave trajectory intersects the detonation wave.

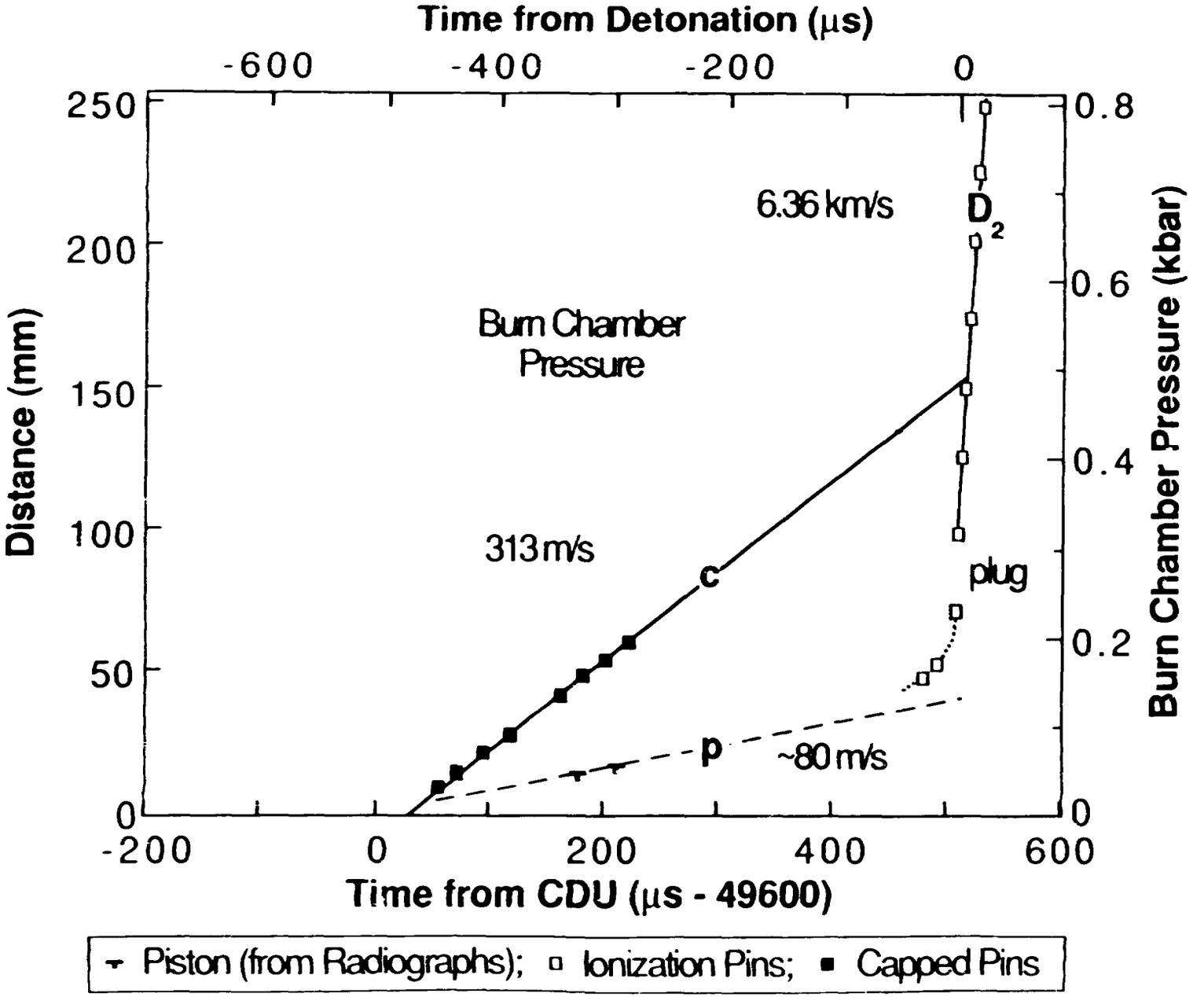
Time from Detonation (μs)
-600
-400
-200
0
250
200
150
100
50
0
0.8
0.6
0.4
0.2
0
Distance (mm)
Burn Chamber Pressure (kbar)
6.36 km/s
D2
Burn Chamber Pressure
313 m/s
c
plug
p
~80 m/s
-200
0
200
400
600
Time from CDU (μs - 49600)
Piston (from Radiographs); Ionization Pins; Capped Pins

This is a time-expanded plot of the data on the previous viewgraph. There are several points of interest.

The lowest three pins describe the ignition front. The third and fourth pin cannot be connected by any single wave because the apparent velocity between them is an unphysical 11 km/s. Therefore, different phenomena must have triggered these pins.

Pins 4-6 describe a velocity of 8.19 km/s. This is very close to the detonation velocity characteristic of 90% TMD HMX. Thus the transition to detonation occurred behind the compaction wave in the 90% material.

Pins 7-10 describe a velocity of 6.36 km/s. This is the characteristic detonation velocity of ~65% TMD HMX. The change of detonation velocity occurred (to the resolution of the experiment) at the point where the extrapolated compaction wave intersects the original detonation.

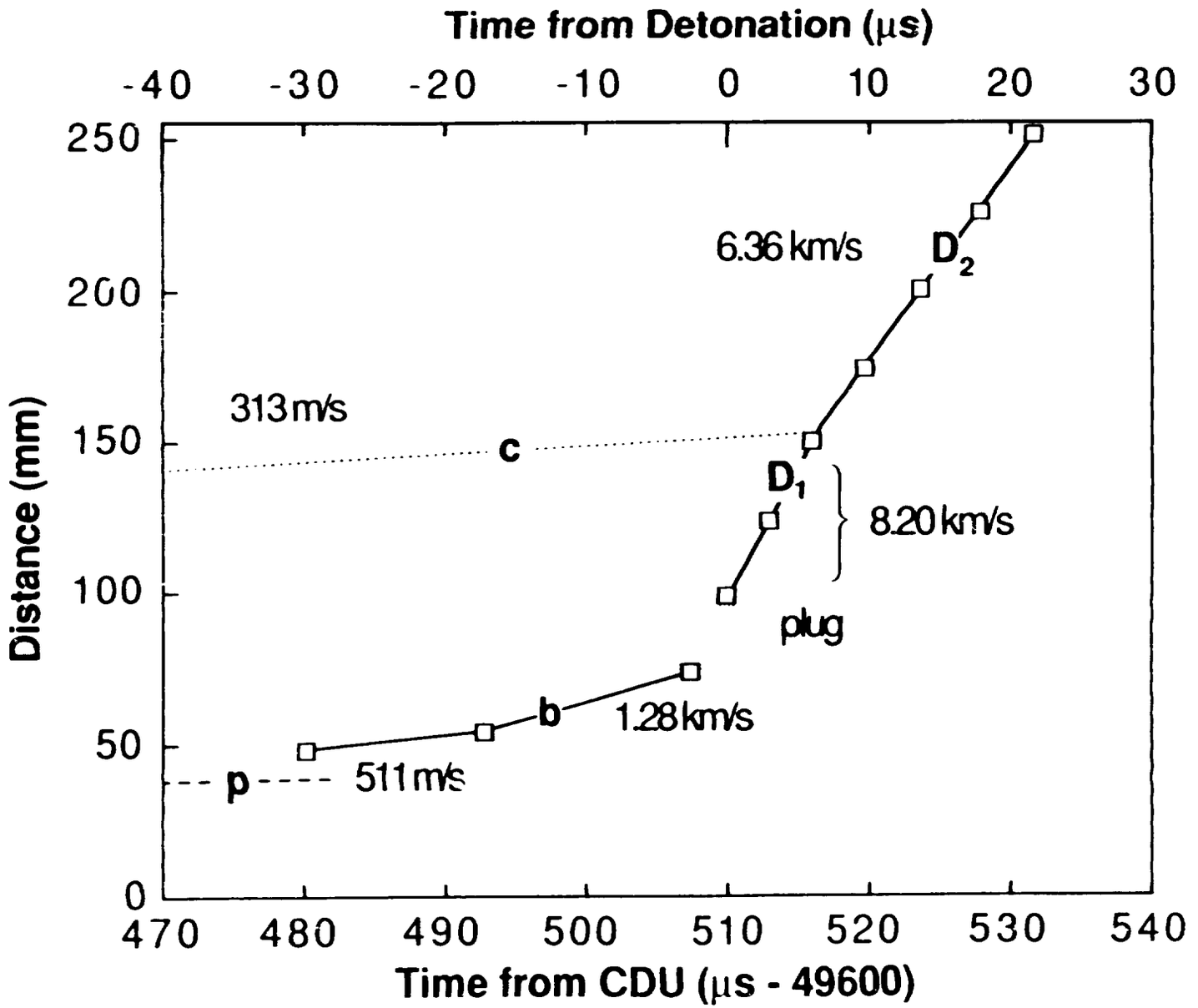
Time from Detonation (μs)
-40
-30
-20
-10
0
10
20
30
250
200
150
100
50
0
Distance (mm)
6.36 km/s
D2
313 m/s
c
D1
8.20 km/s
plug
b
1.28 km/s
p
511 m/s
470
480
490
500
510
520
530
540
Time from CDU (μs - 49600)

Next is a photograph of an experiment fired in a much thicker-walled tube. This test was lit with the Ti + B ignitor system, not a piston. The variations in the wall markings and metal shear patterns are explained by our description of the DDT process.

Below the light band (which will serve as a point of reference), the walls are black with soot deposits. The original machining marks are visible in this portion of the tube. This is the burning region.

The light band has no black deposits, therefore not much HMX was burned before the tube rupture. The dynamic-shear characteristics exhibited in the upper part of the tube begin in this light-band region. This is indicative of a sudden increase in pressure (a shock). The light band is the plug region, which is essentially a shock.

The remaining portion of the tube has marks and deposits that are characteristic of detonation.

The transition to detonation does not have to occur in a single step. This radiograph shows a static and two dynamic pictures.

The first dynamic radiograph shows the now familiar compression of material.

The second dynamic radiograph shows two regions of compressed foils behind the conical distortion caused by the detonation. These radiographs are analyzed in the following viewgraph.

STATIC

FIRST DYNAMIC

SECOND DYNAMIC

SHOT NO. F-5408

These are the density analyses of the two dynamic radiographs. The original bed density was ~75% TMD.

Plot a shows (from the piston) a lower density burning region, a plug from ~53 to ~67 mm, and a 90% compaction in front of the plug to ~86 mm. Thus, the plug-shock was formed, but did not result in a detonation.

Plot b shows the situation after detonation. The detonation front is at ~170 mm. From the piston end, there is a burn region (to ~58 mm), the residual of a plug (~58-72 mm), another burn region (~72-83 mm), a second plug (~83-108 mm), and the expansion of the detonation products (~108-170 mm).

This shows detonation was initiated only after the formation of the second shock.

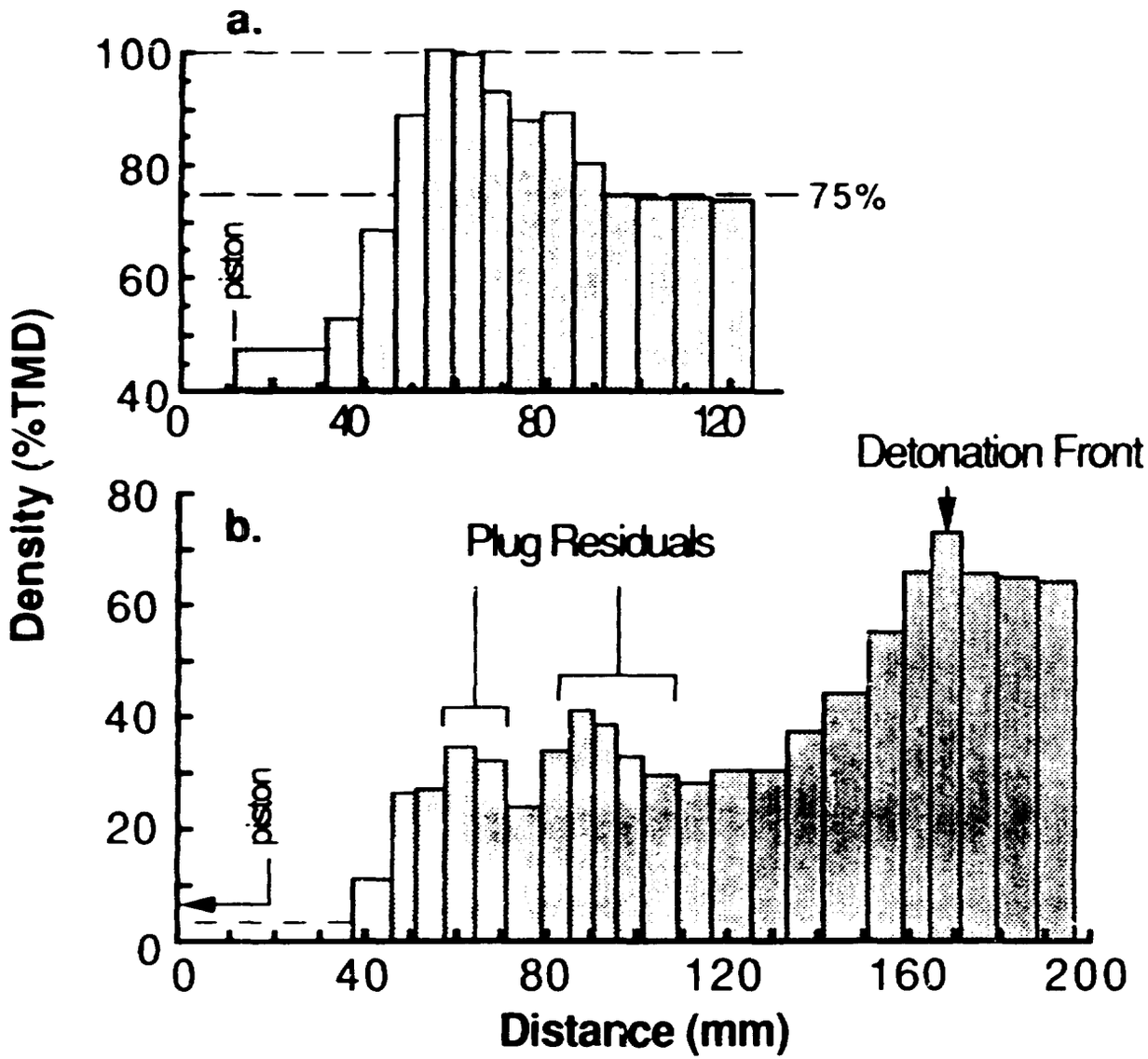
a.
100
80
60
40
75%
piston
0
40
80
120
Density (%TMD)
b.
Plug Residuals
Detonation Front
80
60
40
20
0
piston
0
40
80
120
160
200
Distance (mm)

This viewgraph is a schematic t-x representation of the previous experiment.

The process proceeds according to the previously described mechanism forming shock S_1. However, when this shock overtakes the compaction wave c_1, it is not strong enough to initiate detonation.

The resultant wave from the collision of S_1 and c_1 is a second compaction wave c_2. The normal scenario repeats with the contact surface cs at the top of **Plug #1** behaving like a piston. The resulting shock S_2 is strong enough to initiate detonation.

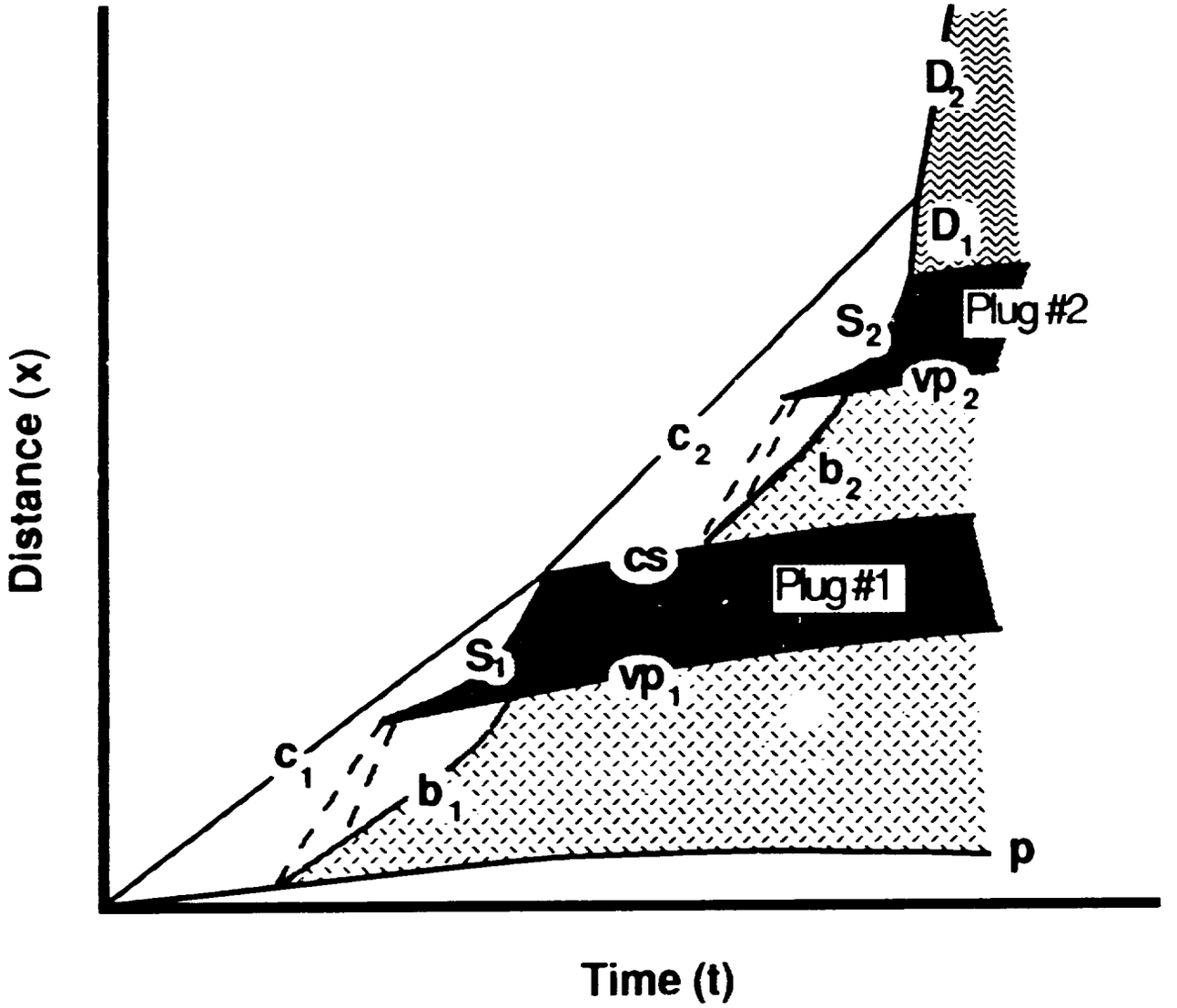
Distance (x)
Time (t)
D2
D1
Plug #2
S2
vp2
c2
b2
cs
Plug #1
S1
vp1
c1
b1
p

This viewgraph shows ali the pin and radiographic data for the two-shock experiment.

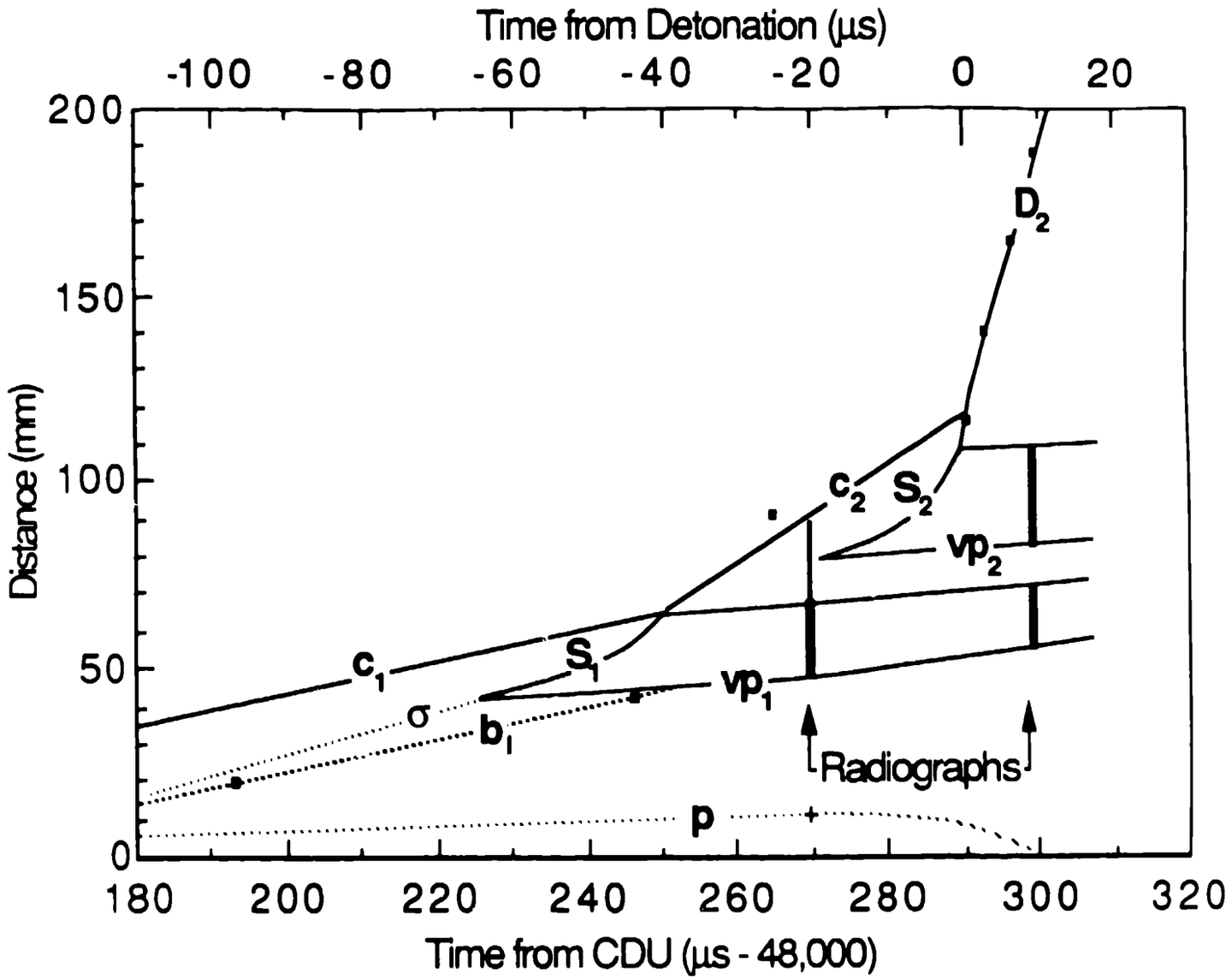

▪ Capped Pins; ‖ Plug (Fig. 14); | 90% Compaction (Fig. 14)
Note: The velocities of the waves (m/s) were measured or estimated according to the following: D_2 = 7053 (pins); **p** = ~75 (radiograph Fig. 14); **b** = 454 (pins); σ =~550 (calculated from Hugoniot); c_1 < 454 (parallel to b at early times); c_2 =~1300 (radiograph and Hugoniot shock match); vp_1 =~75 (same as piston); vp_2 =~130 (Hugoniot shock match)

A further example of multiple shock formation is shown in this figure taken form Smith (1974). A series of confinement failures is evident. These are the consecutive burn regions. This particular detonating cord never reached detonation.

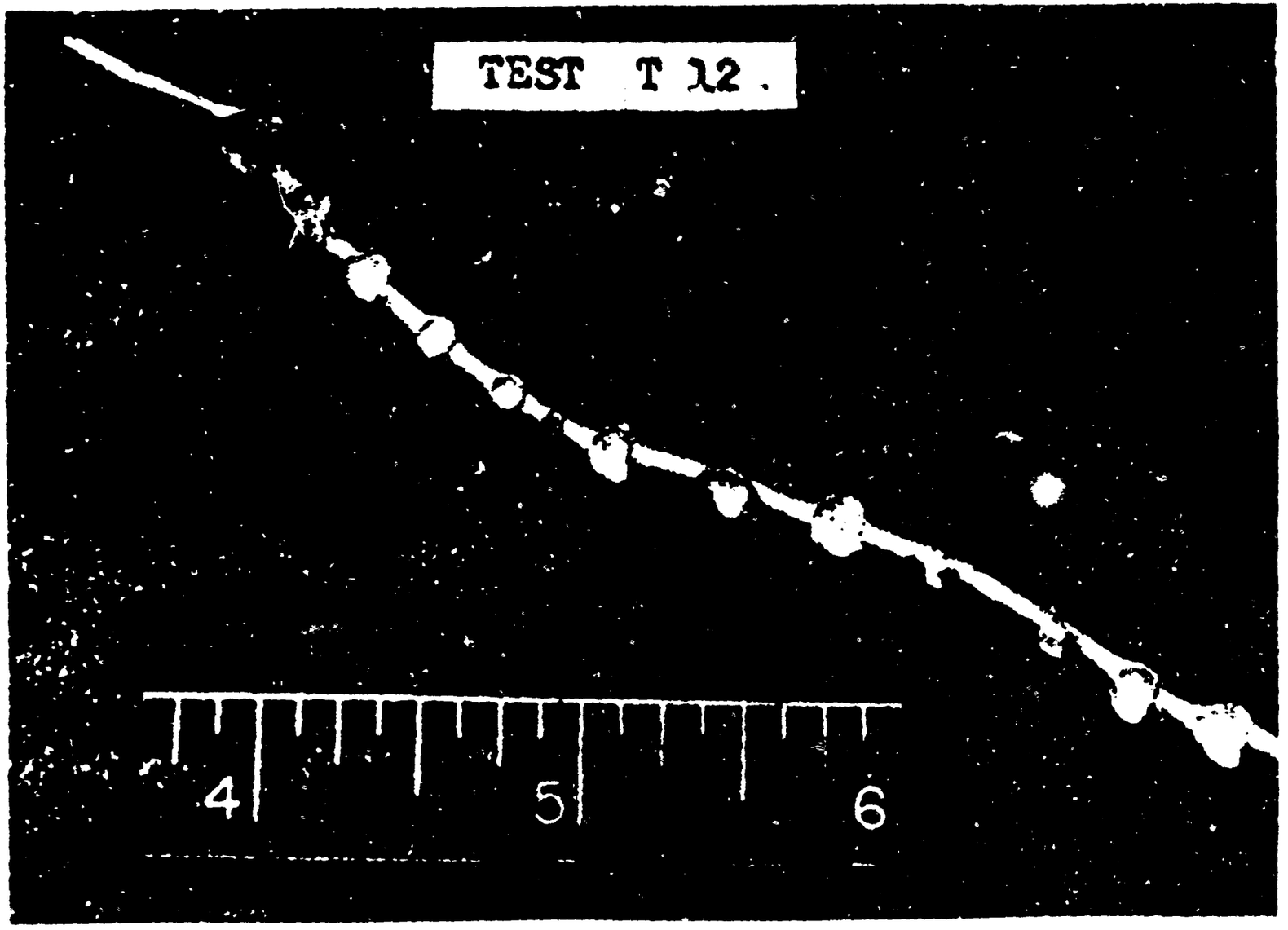
TEST T 12.
4
5
6

The first two conclusions are just a summary of the current exposition. The third conclusion is an assertion based on many analyses of others' data that are not presented here.

CONCLUSIONS:

Burning to detonation is discontinuous

Shock is formed above the burning region

Transition to detonation is by shock initiation

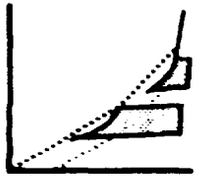

Multiple shocks may form before detonation

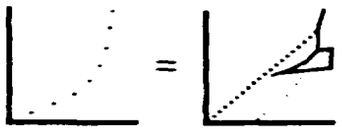

Mechanism is consistent with other worker's experiments

The next several viewgraphs review the application of autocatalytic kinetics to the description of the DDT process. The purpose is to more thoroughly motivate the argument presented earlier concerning the stress-induced acceleration of the ignition wave.

The thermal decomposition of HMX and other nitramines is autocatalytic. The first equation is representation of the chemical equation of the decomposition of species **A** to Species **X** and others. The rate of decomposition R is proportional to both the reactant and product concentrations. In these equations a and x are the instantaneous concentrations of reactant and product, k is the rate constant, a_0 and x_0 are the starting concentration of reactant and product, and t is time.

The earlier discussion of the compaction wave indicated that some small amount of product is produced by the shearing and friction caused by the compaction wave. In this model, we assume that the concentration of product due to this compaction x_0 is directly proportional to the stress level of the compaction σ_c.

HMX Thermal Decomposition is Autocatalytic

$$\mathbf{A} \rightarrow \mathbf{X} + \ldots$$

$$R = \frac{dx}{dt} = kax = k\,(a_o - x)(x + x_o)$$

Initial Product, x_o
generated from compaction-wave stress

$$\sigma_c \Rightarrow x_o$$

This viewgraph shows particular features of the autocatalytic rate equation. Three rate are defined: The maximum rate R_{max}, the rate at which there are points of inflection in the curve R', and the rate marking the beginning of fast reaction R_τ. The width of the rate curve is noted as Δkt.

R_τ is calculated by extrapolating a line of slope dR/dt through the point (R', t') to the abscissa. This intersection is τ. The rate corresponding to τ is R_τ.

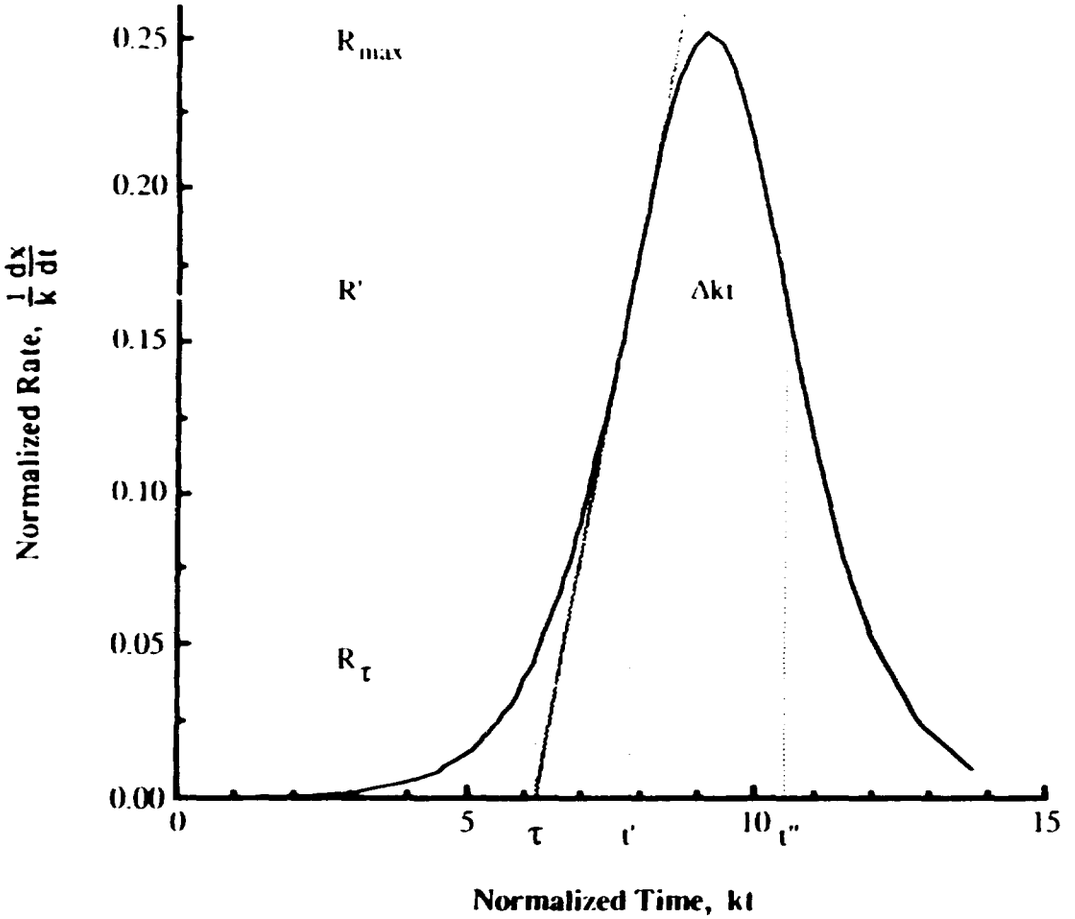

Los Alamos

DYNAMIC TESTING DIVISION

This viewgraph shows the effect of changing the initial concentration of product on the rate. The overall shape and width does not change significantly. However, the time of the peak rate moves with x_o. The dependence appears logarithmic.

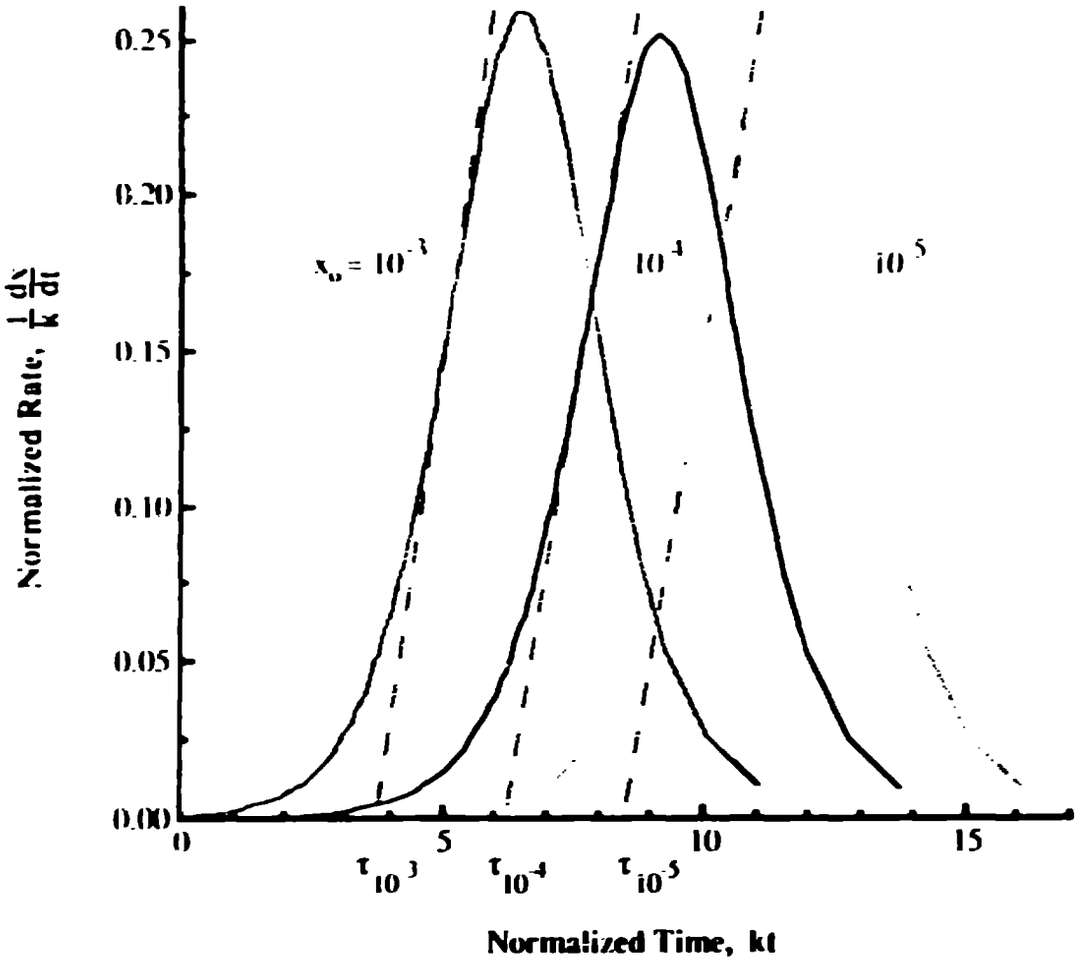

Los Alamos
DYNAMIC TESTING DIVISION

Detailed analysis of the rate equation and the assumptions listed show that the induction time τ is dependent strictly on the rate constant and the initial-product concentration.

Induction Period

Depends on

Initial Product Concentration

if $x_o \ll 1$ and $a_o = 1$

$$k\tau = \ln\left[\frac{\left(\frac{1}{2} - \frac{\sqrt{3}}{6}\right)}{\left(\frac{1}{2} + \frac{\sqrt{3}}{6}\right) x_o}\right] - \frac{\sqrt{3}}{k} \approx \ln \frac{0.0474}{x_o}$$

if $k = 1$

Integration of the rate equation and a definition of pressure based on void volume and the ideal gas law shows that the rapid rise in interstitial pressure is well represented by τ. Φ_0 is 0.10 in this calculation.

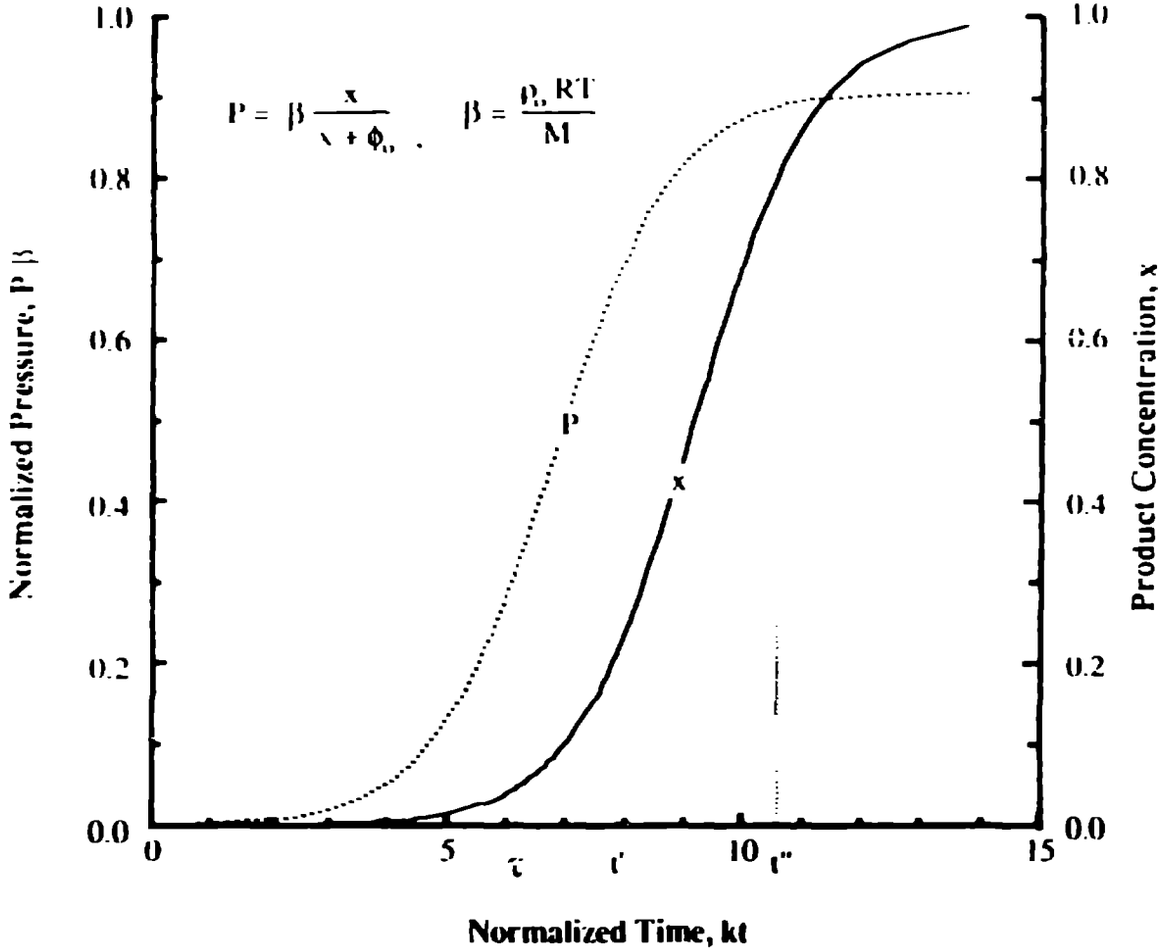

Los Alamos

DYNAMIC TESTING DIVISION

This formalism is applied to the DDT model by noting that if the compaction wave produces a concentration of product x_0, then additional stress above σ_c should produce additional product x_s. The rate equation can be rewritten as shown to include this additional stress-produced product.

Comparing the pressure (stress) dependent rate equation to the simple rate equation shows that the rate is increased by a multiplicative factor to the initial product concentration.

Application to DDT

Stress-Produced Product:

Compaction Wave - $\sigma_c \Rightarrow x_o$

Stress Waves - $\sigma_i \Rightarrow x_s$

Addition in Rate Equation:

$$\frac{dx}{dt} = k\,(a_o - x - x_s)(x_o + x + x_s) \approx k\,(a_o - x)(x + \frac{P}{\sigma_c} x_o)$$

$$\frac{dx}{dt} = k\,(a_o - x)(x + x_o)$$

The increase rate caused by additional stress after the compaction wave shortens the time it takes to reach the rate that defines the induction period. Therefore, the ignition wave accelerates relative to the compaction wave.

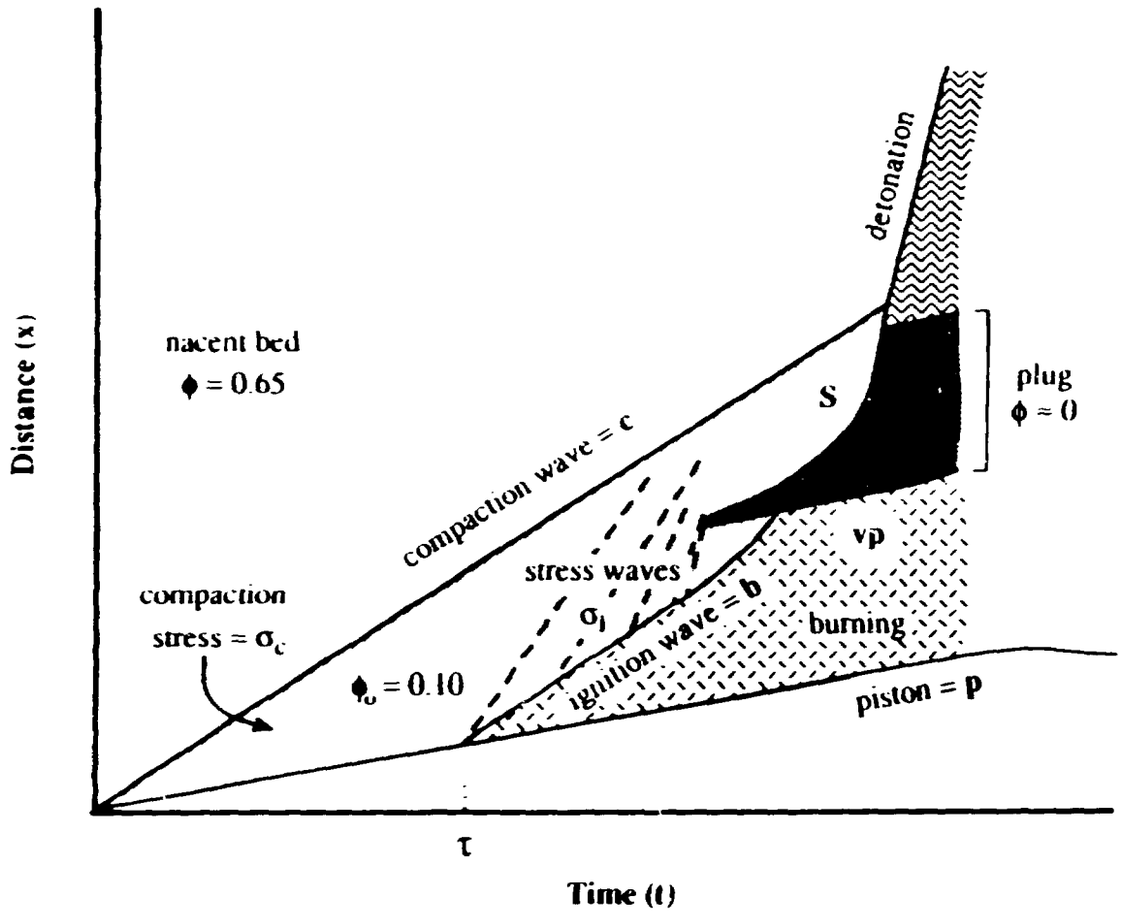
Distance (x)
nacent bed
$\phi = 0.65$
detonation
plug
$\phi = 0$
S
compaction wave = c
stress waves
σ_i
vp
burning
ignition wave = b
compaction
stress = σ_c
$\phi_o = 0.10$
piston = p
τ
Time (t)